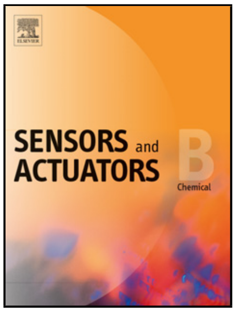

GENERATION OF GRAPHITE NANOMATERIALS FROM PENCIL LEADS WITH THE AID OF A 3D POSITIONING SPARKING DEVICE: APPLICATION TO THE VOLTAMMETRIC DETERMINATION OF NITROAROMATIC EXPLOSIVES

Maria G. Trachioti (Investigation) (Writing - original draft), Dusan Hemzal (Data curation) (Formal analysis), Jan Hrbac (Writing - review and editing), Mamas I. Prodromidis (Conceptualization) (Supervision) (Funding acquisition) (Writing - review and editing)

PII: S0925-4005(20)30218-5

DOI: https://doi.org/10.1016/j.snb.2020.127871

Reference: SNB 127871

To appear in: *Sensors and Actuators: B. Chemical*

Received Date: 15 November 2019

Revised Date: 11 February 2020

Accepted Date: 13 February 2020

Please cite this article as: Trachioti MG, Hemzal D, Hrbac J, Prodromidis MI, GENERATION OF GRAPHITE NANOMATERIALS FROM PENCIL LEADS WITH THE AID OF A 3D POSITIONING SPARKING DEVICE: APPLICATION TO THE VOLTAMMETRIC DETERMINATION OF NITROAROMATIC EXPLOSIVES, *Sensors and Actuators: B. Chemical* (2020), doi: https://doi.org/10.1016/j.snb.2020.127871

GENERATION OF GRAPHITE NANOMATERIALS FROM PENCIL LEADS WITH THE AID OF A 3D POSITIONING SPARKING DEVICE: APPLICATION TO THE VOLTAMMETRIC DETERMINATION OF NITROAROMATIC EXPLOSIVES

Maria G. Trachioti[1], Dusan Hemzal[2], Jan Hrbac[3], Mamas I. Prodromidis[1,*]

[1] Department of Chemistry, University of Ioannina, Ioannina 45110, Greece
[2] Department of Condensed Matter Physics, Masaryk University, 611 37 Brno, Czech Republic
[3] Department of Chemistry, Masaryk University, 625 00 Brno, Czech Republic

*Corresponding author: Tel: +30 26510 08301; E−mail: mprodrom@uoi.gr

Graphical abstract

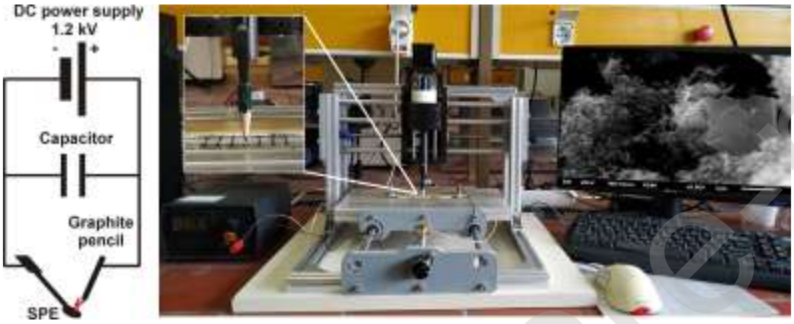

Highlights

- 3D−sparking head aided in−situ tailoring of the electrode surface by graphite pencil
- Generation of sponge−like graphite nanostructures and 2D few−layer graphite flakes
- Fabrication of low-cost semi-disposable sensors for 2,4,6-trinitrotoluene (TNT)
- Cathodic determination of TNT allows an LOD as low as 0.44 ppb
- Anodic determination of TNT offers an LOD of 0.25 ppb in non-deoxygenated solutions

Abstract

We report on facile generation of graphite nanomaterials (GNMs) with advanced electro catalytic properties through a direct electric discharge process between pencil leads and graphite screen−printed electrodes (SPEs) at ambient conditions at 1.2 kV. Various commercially available pencil leads of different degrees of hardness were examined. Sparked GNM−SPEs were characterized by Raman spectroscopy, SEM, CV, and EIS. Taking as criterion the highest response to the electro-reduction of nitro group of 2,4,6−trinitrotoluene (TNT) at −0.3 V at deoxygenated solutions, Castell 9000 (2B) pencil was selected as optimum. GNM−SPEs exhibited a linear response over the concentration range 1−100 ppb TNT, while the limit of detection (LOD) based on the 3σ/m criterion was calculated 0.44 ppb. The interference effect of other nitro−aromatic explosives and masking compounds, which are used to hinder the detection of TNT, was extensively investigated. The determination of TNT was also achieved by measuring the oxidation of the electrochemically generated hydroxylamine groups. In this format, each measurement was conducted with a new electrode polarized at −0.275 V for 2 min. At the cost of a slightly increased time of analysis, the anodic determination of TNT offered increased selectivity, applicability in non−deoxygenated solutions, linear response over the concentration range 1−50 ppb TNT and an LOD of 0.25 ppb. GNM−SPEs were successfully applied to the determination of TNT in spiked drinking water samples. Recovery was 101−108%.

Keywords: electric discharge; carbon nanomaterials; sparking; 2,4,6−trinitrotoluene; screen−printed electrodes

1. Introduction

Trace detection of energetic explosive compounds, such as nitro-aromatic compounds, is of great importance for a broad range of applications including forensic analysis, civilian and airport security, military and defense purposes, environmental monitoring [1,2], etc.. Among various nitro-aromatic compounds, 2,4,6−trinitrotoluene (TNT) has attracted the highest popularity due to its widespread use as an explosive material for military, industrial, and mining applications, which, in turn, has resulted in significant levels of soil and groundwater contamination. Environmental protection agency (EPA) has assigned TNT to be a possible human carcinogen (weight−of−evidence carcinogenic classification of C), while also having been included in the latest EPA's report of compounds causing cancer or reproductive toxicity [3]. For TNT in drinking water, EPA has calculated a risk-based carcinogenic screening level of 2.5 ppb [4].

Therefore, development of analytical methods for sensitive, selective and accurate determination of TNT is highly desirable. Among the various techniques which have been used for the determination of explosive compounds, electrochemical−based methods exhibit certain advantages associated with intrinsic features of electrochemical transducers, such as low−cost, portability, sensitivity and the ability to be incorporated in modern formats of detection instruments, such as wearable/balloon/finger-based devices [5–8].

Electrochemical determination of TNT has been conducted through the electro-reduction of the –NO_2 groups in the aromatic ring. This approach has led to the development of methods with attractive detection capabilities by employing electrodes modified with rather complex nanomaterials based on metal nanoparticles [9–11], carbon−based nanostructures [12–19] or hybrid metal/carbon−based electrocatalysts [20–23]. Even though some of these methods offer LODs at the ppb level, they suffer from i) laborious and lengthy protocols for the preparation of the nanostructures, ii) use of costly reagents for the synthesis of noble metal nanoparticles, and iii) the necessity of preparing fresh batches of the designed nanomaterials in order to ensure a good reproducibility among sensors fabricated at different time intervals. The latter issue results also in the production of high waste loadings as well as in an increased cost per sensor and per analysis [9–11,20,22].

Intrinsically, the cathodic determination of TNT, through the electro-reduction of the –NO_2 groups cannot ensure sufficient selectivity against other nitro aromatic compounds. Selectivity is based on the (different) –NO_2 group(s) in the aromatic ring being reduced at different potentials depending both on the number of –NO_2 groups and their position in the aromatic ring (*ortho*, *meta* or *para* position). In this regard, TNT exhibits three reduction peaks, with the one positioned at the least cathodic potential used for the discrimination of TNT over other mono− or dinitro aromatic compounds. However, in the excess of other dinitro compounds (mostly of 2,4−dinitrotoluene (2,4−DNT)) the peaks overlap. In order to achieve higher selectivity against other nitro compounds, various biorecognition elements have been employed. Zhang et al. proposed a smartphone−based device utilizing graphite screen−printed electrodes (SPEs) modified with TNT specific peptides [24], which however showed low selectivity against 2,4−DNT, generating a response of about one third of that to TNT. Shahdost−Fard and Roushani [23] proposed a device based on a TNT−binding aptamer immobilized on the surface of a glassy carbon electrode (GCE), which at the cost of a lengthy incubation step of 30 min showed high selectivity to TNT.

Another issue related to the electro-reduction of the –NO_2 group is oxygen interference, a common obstacle in cathodic voltammetric measurements in which the large background signal due to the electro reduction of dissolved oxygen, hinders the detection of TNT even at high concentrations. Indeed, the voltammetric determination of TNT at gold electrodes modified with self−assembled monolayers containing aromatic compounds, which have been found to suppress the electrochemical reduction of dissolved oxygen, resulted in LODs higher than 500 ppb TNT [25]. Similarly, an LOD higher than 2000 ppb was achieved with carbon electrodes modified with TiO_2/metal nanoparticles applied to the cathodic determination of TNT in non−deoxygenated solutions [11].

To address the afore−mentioned limitations we propose a method comprising certain advantages regarding the fabrication of the electrodes, the modification of their surface, and the assay protocol for the electrochemical determination of TNT. Specifically: a) sensors are based on low−cost, semi−disposable graphite SPEs, b) SPEs were modified with a 3D−sparking head aided SPE−to−graphite pencil in−situ tailoring process. This process offered highly reproducible sensors at an extremely low cost, within a few minutes and in the absence of any liquids or costly reagents. Raman studies demonstrated development of sponge−like graphite nanostructures and low dimensional few−layer graphite flakes endowing outstanding electrocatalytic properties towards the electrochemical determination of TNT at the sub−ppb concentration level, c) TNT was determined by applying cathodic measurements at deoxygenated solutions as well as anodic measurements at non−deoxygenated solutions by measuring the oxidation of the electrochemically generated hydroxylamine groups at electrodes that have been priory polarized at −0.275 V for 2 min, and d) both cathodic and anodic electroanalytical formats were successfully applied to the determination of TNT in spiked drinking water samples.

2. Experimental section

Materials

Mechanical pencil leads (HB hardness, 0.7 mm thickness) were purchased from Pilot (“high−purity graphite leads”, ENO−G), and Uni-ball (“needle−crystal leads”, Uni and “nanodiamonds leads”, Nano−Dia), while graphite pencils of different hardness (4H, 2H, HB, 2B, 4B) were products of Faber−Castell (Castell 9000). TNT stock solution [1 mg mL^{-1} in acetonitrile (ACN)] was obtained by Cambridge Isotope Laboratories, Inc. 2,4−dinitrotoluene (2,4−DNT), 2,6−dinitrotoluene (2,6−DNT), 2−nitrotoluene (2−NT), 4−nitrotoluene (4−NT) and caffeine were purchased from Aldrich, 3−nitroaniline (3−NA) from Ferak Berlin, nitrobenzene (NB), D−glucose and acetylsalicylic acid from Sigma−Aldrich, ACN from Riedel−de Haen and sodium dihydrogen phosphate monohydrate, potassium chloride, hexacyanoferrate(II)/(III) from Merck. Stock solutions of nitro−aromatic compounds were prepared in ACN, while diluted working solutions were prepared in 0.1 M phosphate buffered saline (PBS), pH 7 and were stored at 4 ^{o}C. Double distilled water (DDW) was used throughout.

2.2 Apparatus

Electrochemical measurements (cyclic voltammetry, CV; differential pulse voltammetry, DPV; electrochemical impedance spectroscopy, EIS) were conducted with a PGSTAT12/FRAII electrochemical analyzer (Metrohm Autolab) in a conventional 3−electrode cell. Plain or spark-modified SPEs were used as the working electrode. A Pt wire served as the auxiliary electrode and the reference electrode was a Ag/AgCl/3M KCl (IJ Cambria) electrode and all potentials reported hereafter are cited to the potential of this electrode. DP voltammograms were recorded in 0.1 M PBS, pH 7 using the following parameters: modulation amplitude: 0.05 V, step potential: 0.006 V, modulation time: 50 ms, interval time: 200 ms. CV experiments were conducted in 0.1 M PBS, pH 7 containing 5 mM hexacyanoferrate(III) at a scan rate 0.050 V s$^{−1}$. EIS measurements were conducted in a mixture of 5+5 mM hexacyanoferrate(II)/(III) in 0.1 M PBS, pH 7 over the frequency range from 100 KHz to 0.1 Hz by using a sinusoidal excitation signal of 0.010 V (rms). The applied DC potential value was 0.200 V. Data simulation to an equivalent electric circuit was performed with the FRA 4.6 software (Metrohm Autolab). Scanning electron microscopy (SEM) images were taken with a JEOL JSM−6510LV microscope equipped with an INCAPentaFETx3 (Oxford Instruments) energy dispersive X−ray (EDX) spectroscopy detector. Raman spectra were collected using Renishaw inVia micro−Raman system and ×50 lens with beam−expander in ambient conditions. The diffraction−limited spot size was 1 µm for 200 µW DPSS laser at 532 nm by Coherent. Exposure for all spectra was set to 10 s. Raman spectra were collected at plain SPE, sparked SPE and on spark extracted carbon flakes on the SPE substrate (polyester foil). Imaging data were extracted from Raman intensities at three channels: 1560−1600 cm$^{−1}$ for G band (red channel), 1300−1400 cm$^{−1}$ for D band (blue channel) and 2680−2760 cm$^{−1}$ for 2D band (green channel). Prior to processing, the spectra at plain and sparked graphite surface were background−corrected for luminescence. Spectra on the spark-extracted graphite flakes were additionally corrected for the polyester foil bands (1600−1630 cm$^{−1}$ in the gray channel, 1720−1740 cm$^{−1}$ in the blue channel and 1450−1470 cm$^{−1}$ in the green channel (Fig. S1).

2.3 Modification of SPEs by sparking process

Modification of graphite SPE (203 sparking cycles, unless stated otherwise) was performed by connecting the graphite pencil as cathode (−) and graphite SPE as anode (+) to an in−house power supply and bringing, through a G−code controlled 3D positioning device, the two materials into close proximity until the spark discharge occurred at 1.2 kV DC at ambient conditions. An external capacitor (2.8 nF) was connected in parallel to the power supply output terminals. **Fig. S2** illustrates the block diagram and the experimental setup for the sparking process. For comparison purposes, graphite SPEs were also modified with graphite pencils (Faber−Castell, Castell 9000, 4H−4B hardness) and mechanical pencil leads (Pilot, Uni−ball). Details on the highly reproducible automatic sparking process with the aid of a 3D positioning device and on the fabrication of the graphite SPE on flexible polyester sheets are given in Refs [26] and [27], respectively.

2.4 Measurement procedure

Cathodic determination of nitro compounds: Modified SPEs were immersed in a 20−mL vial containing the calibrants or the samples and the supporting electrolyte (0.1 M PBS, pH 7). The measuring solution was deaerated for 15 min with N_2. A deposition step at –0.1 V took place for 30 s under stirring and a cathodic voltammetric scan was performed from –0.1 to −0.75 V, after an equilibration period of 10 s. The concentration of TNT was calculated by registering the peak current at ca. –0.3 V. Drinking water samples were analyzed by following the same measurement protocol using the standard addition method.

Anodic determination of nitro compounds: Modified SPEs were polarized at −0.275 V for 2 min in non−deoxygenated solutions (0.1 M PBS, pH 7) under stirring aiming at the electro-reduction of the $–NO_2$ group to hydroxylamine (NH−OH). After an equilibration period of 10 s, an anodic scan from −0.275 to 0.25 V was conducted in order to measure the oxidation current of the electrochemically generated hydroxylamine to the respective nitroso compound NH−OH/(–NO) at ca. 0.025 V. In this format, each measurement was conducted with a new electrode.

3. Results and discussion

3.1 Optimization of the sparking process

Various graphite pencil (Castell 9000) and mechanical pencil leads **(**ENO−G, Uni, and Nano−Dia), all at a degree of hardness HB, were preliminary examined as different graphite sources for the modification of the SPEs surface with 100 sparking cycles at 1.2 kV under ambient conditions. Taking as criterion the efficiency of the resulting sparked−SPEs to the electro reduction of TNT (**Fig. S3**), Faber−Castell pencil was selected as optimum. Graphite pencils and leads are consisted of three components: graphite (41-90% w/w), clay (53-4% w/w) which is used as a binder to increase the tolerance (hardness), and wax particles at about 5% w/w [28]. As a result, graphite pencils of different hardness differ in both composition and conductivity (**Table S1**) and thus hardness is expected to affect the sparking parameters and the electro-catalytic efficiency of the resulting sparked surfaces. Among SPEs sparked with 4H, 2H, HB, 2B and 4B pencils, 2B gave the best results (**Fig. S4**). Finally, the effect of the sparking cycles on the electro-reduction of TNT was examined by comparing the reduction peak currents at −0.3 V of SPEs modified with 2B Faber−Castell pencil with 52, 81, 100, 152, 203, 255 and 300 sparking cycles. The highest response was obtained after 203 sparking cycles (**Fig. S5**).

3.2 Morphological characterization

SEM images illustrated in **Figs. 1A, B** revealed the formation of sponge−like graphitic surfaces along with regions rich in low dimensional few−layer graphite flakes. Compared with the relatively featureless surface of the plain graphite SPEs (**Fig. S6**), both of the sparking process−induced surface morphologies can potentially enhance the electro catalytic properties of the resulting SPEs as i) sponge−like nanostructures increase the electro active surface and ii) low dimensional few−layer graphite flakes resemble greatly graphene structures that cause lowering of the electric resistance of the electrode surface and facilitate electron transfer phenomena. In addition, planar graphitic surface rich in π−electrons is expected to increase the affinity of the surface to various aromatic (as for example the target analyte) compounds. As regards the origin of graphene−like flakes, i.e. whether they occurred by spark−induced structural transformation of the basal graphite ink or they represent spark−exfoliated material, EDX mapping reveals a composite material, similar to the graphite pencil (**Table S1)**, with silicon atoms, colored in pink, to represent the clay fraction.

3.3 Raman imaging studies

Raman fingerprints of basic graphite forms have been extensively described [29]. A good quality bulk graphite is characterized by strong G band, weak 2D band, and as small intrusion of D band as possible. On the other hand, poor quality bulk graphite is characterized by strong G band, weak 2D band, and a considerable amount of D band. Finally, a few−layer graphite is characterized by G and 2D bands of comparable intensities, with negligible intrusion of D band. In particular, graphene requires the 2D band being stronger than G band and shifted to lower wavenumbers.

The blue, red and green channels of the Raman maps presented in **Fig. 2** correspond to carbon D−, G− and 2D bands, respectively, which together form a convenient indicator of the carbon condition. The extent of individual bands is shaded, while carbon color coding is the same for all three samples to allow direct comparison.

Raman spectra of the plain electrode show variability in condition of the contained carbon in the range of low−quality graphite. However, two main changes can be identified after sparking: significant increase of D band and emergence of a pronounced 2D band, while both contributing to the blue−shifting of the sparked Raman map. These alterations can be correlated with sparking-induced disorder of the graphite. While certain spectra suggest sparking−induced introduction of higher quality carbon areas through the emergence of sharper features within the Raman bands (cf. sparked trace 3 in **Fig. 2B**), this effect is generally masked by the intrinsic carbon content background of the whole electrode. In this regard, Raman imaging experiments were also conducted on a spark−extracted graphite flake over the electrode substrate. Due to the flake not having been transferred from the original post-impact sparking site, the average Raman signal coming from the polyester (PES) substrate had to be subtracted (see **Fig. S1**).

Without the intrusion of the background carbon signal, the effect of sparking becomes easily identified in the Raman spectra: the bulk part of the flake exhibits very high disorder, while one of the flake edges exhibits few−layer graphite morphology. Presumably, field enhancement by a graphene-like material could be contributing to SERS efficiency of the sparked electrodes. Additionally, high reactivity of the sparked material was confirmed by the necessity to employ low laser power in order to prevent sample burning.

3.4 Electrochemical characterization

Fig. 3A shows the CVs of two SPEs modified with 43 and 203 sparking cycles along with a plain SPE, which was used for comparison at 0.1 M PBS, pH 7 containing 5 mM hexacyanoferrate(III). GNM−SPEs exhibited considerable lower separation peak potential ($\Delta E_{p(43)}$=244 mV; $\Delta E_{p(203)}$=286 mV) compared with that observed at the plain electrode (ΔE_p=711 mV), and higher redox peaks with both anodic and cathodic currents proportional to the number of the sparking cycles.

For further exploration of electro-catalytic properties at the sparked electrode/electrolyte interface faradic EIS measurements were conducted and are presented as Nyquist plots in **Fig. 3B**. As has been analyzed in detail in previous works of our group [26,30], impedimetric data at the sparked surface/electrolyte interfaces, in the low frequency region, cannot be sufficiently modeled by a single Warburg element. Similarly, EIS data at GNM−SPE were simulated by a modified Warburg element incorporating a constant phase element (CPE) connected in parallel that accounts for the extended surface roughness caused by electric discharge phenomena during the modification process. Interestingly, in the high frequency region both of the sparked electrodes exhibited a single semicircle. This behavior was anticipated for the SPE that had been modified with 203 sparking cycles, but was unexpected for the one modified with only 43 sparking cycles [26], as for the latter the sparking process has not been applied across the entire surface of the electrode. In this case, the electrode surface is characterized by two different interfaces with the electrolyte; those rich with the spark generated nanoparticles (sparked regions) and the rest of the electrode surface which either contains lesser amount of sparked nanoparticles or is even plain. These different interfaces are characterized by different time constants ($\tau=1/RC$) which result in appearance of two (partially overlapped) semicircles. The emergence of a single semicircle at both examined sparked electrodes (43 and 203 sparking cycles) can be explained considering that carbon is the major component at both the sparking tip electrode (graphite pencil) and the substrate (graphite SPE). We note, however, that based on the values of the R_s and R_{ct} at the two examined sparked electrodes, the higher number of sparking cycles resulted in a higher electro catalytic activity, $R_{ct(43)}>R_{ct(203)}$. However, $R_{s(43)}<R_{s(203)}$ indicates that the sparking process might cause damage to the electrode surface.

3.5 Electro catalytic performance and selectivity of electrodes based on the electro reduction of nitro group

DP voltammograms in **Fig. 4** show that sparked GNM−SPEs offer a suitable surface for the electro reduction of various nitro-aromatic compounds, such as 2−NT, 4−NT, 2,6−DNT, 2,4−DNT and TNT by providing one reduction peak for each nitro group in the molecule. Specifically, mono nitro compounds (2−NT, 4−NT) possess a single reduction peak, dinitro compounds (2,6−DNT, 2,4−DNT) possess two reduction peaks, and TNT possesses three peaks. These data along with the position and the height of the peaks led to three conclusions: a) each peak corresponds to the reduction of a particular nitro group and not to the progressive reduction of nitro group(s) collectively to the respective amine derivatives, as mentioned in previous works [7,21], b) the position of each peak is dependent on the number and the position of the other nitro group(s) in the molecule. Data show that there is not a fixed position for the nitro groups at the *ortho*− (2− or 6−) or the *para*− (4−) positions. Based on previous works [31,32], the first two peaks during the cathodic scan of TNT are attributed to the nitro groups at the ortho positions with respect to the methyl group, which as +*I* effect group acts as an electron donor to the adjacent nitro groups, and c) TNT only possesses a reduction peak at −0.3 V that can be used for its selective determination against the other examined nitro aromatic compounds. Interestingly, this peak showed the highest current magnitude and, therefore, was selected for quantitative purposes.

The interference effect of various nitro aromatic compounds, such as 2,4−DNT, 2,6−DNT, 4−NT, 2−NT, 3−NA and NB was evaluated by conducting measurements at single solutions containing 25 ppb TNT as well as at mixed solutions containing 25 ppb TNT and up to 100−fold excess of the examined compounds. The interference effect was evaluated by taking as criterion a 10% error in the magnitude of the reduction peak of TNT at −0.3 V. In this regard, 4−NT, 2−NT, 3−NA and NB at a 100−fold concentration excess do not interfere. On the other hand, dinitro compounds, such as 2,6−DNT and 2,4−DNT that exhibit two reduction peaks (**Fig. 4**), showed a lower interference tolerance. At 25− and 50−fold concentration excess they caused a change of the peak height of TNT at −0.3 V of +1.8, −38.4 and −20.9 and −31.8 %, respectively (**Fig. S7**).

The interference effect of other compounds, such as glucose, caffeine and acetylsalicylic acid, which are used as masking agents or because they have similar physical characteristics with TNT was also assessed [9]. At 100−fold concentration excess the interference effect of glucose was nil, while caffeine and acetylsalicylic acid caused a 14% and −13% error on the peak height of TNT at −0.3 V, respectively.

3.6 Electrocatalytic performance and selectivity of electrodes based on the electro oxidation of the electrochemically generated hydroxylamine group

The aim of this study was to explore the possibility to determine the various nitro explosives by measuring the oxidation of the electrochemically generated hydroxylamine to the respective nitroso (R−NO) compound. At the cost of an extra polarization step, which is necessary for the hydroxylamine derivative to be generated, the anodic determination of TNT offers two distinct advantages: a) measurements can be conducted directly in non−deoxygenated solutions, a feature of great analytical importance for applications in the field, and b) there is an increased interference tolerance, as demonstrated below for 2,4−DNT, which had shown the highest interference effect at the cathodic determination of TNT.

The principle behind the achievement of an improved selectivity relies on each nitro group being reduced at a particular potential. As seen in **Fig. 5**, the most reduction susceptible nitro group in TNT is reduced to its respective hydroxylamine at ca. −0.4 V without triggering the simultaneous generation of the respective hydroxylamine derivative of the corresponding reduction susceptible nitro group in 2,4−DNT which would occur at a more cathodic potential (ca. −0.5 V, **Fig. 5**).

Including, for demonstrating purposes, a mono nitro compound (4−NT), CVs illustrated in **Fig. 5** show that each electrochemically generated hydroxylamine is oxidized. In fact each hydroxylamine/nitroso redox transition occurred at a distinct formal potential corresponding to each nitro group existing in the molecule. Data also manifest that the lower the reduction potential of the nitro groups the higher the formal potential of the corresponding –NHOH/–NO redox couple.

As shown in **Fig. 5**, 4−NT gave one reduction peak at −625 mV, which corresponds to the equation $R{-}NO_2 + 4e^- + 4H^+ \rightarrow R{-}NHOH + H_2O$, and a pair of peaks at a formal potential of −79.5 mV, which includes a peak at −71 mV attributable to the oxidation of the electro-generated hydroxylamine to the nitroso−compound according to the equation R−NHOH → R−NO + $2H^+$ + $2e^-$, and during the reversed scan of the potential, a peak at −88 mV, which is assigned to the reduction of the nitroso−compound back to hydroxylamine R−NO + $2H^+$ + $2e^-$ → R−NHOH.

Analogously, 2,4−DNT produced two reduction peaks at −625 mV and −498 mV accompanied by two pairs of redox peaks centered at E^0=−69.5 mV and E^0=9 mV, and TNT produced three peaks at −623 mV, −518 mV and −378 mV accompanied by three pairs of redox peaks positioned at E^0=−69.5 mV, E^0=−5 mV, and E^0=65.5 mV.

All the CVs illustrated in **Fig.5** represent the second scan. During the first scan, at a starting potential of 0 V, the pair of peaks which is assigned to the –NHOH/–NO redox couple did not appear (**Fig. S8**).

Based on the above data, the sensitivity and selectivity of the electrochemical oxidation of TNT depends on the value of the cathodic potential that will be applied for the electrochemical generation of R−NHOH as well as the length of its application. DP voltammograms illustrated in **Fig. 6** demonstrate that for an application period of 10 s, polarization of sparked GNM−SPEs at −275 mV offers excellent selectivity against 2,4−DNT and at the same time a sufficient sensitivity for TNT.

3.7 Analytical performance

3.7.1 Direct electro reduction of TNT

The response of sparked GNM−SPEs at different deposition potentials, −0.1, 0, 0.1 and 0.2 V, in the presence of 20 ppb TNT and at a deposition time 60 s was investigated (**Fig. S9**). With respect to the highest peak height at −0.3 V, a potential value of −0.1 V was selected as optimum. At this potential value, the response of the sparked electrodes at three discrete deposition time intervals of 30, 60 and 120 s was also investigated and a deposition time of 30 s was selected as it offered lower background signals and better linearity at the respective calibration plot.

The repeatability of GNM−SPEs for five successive measurements at 10 ppb and 50 ppb TNT was found to be 7.6% and 1.8%, respectively, while the inter electrode reproducibility among different electrodes was <3% (10 ppb TNT, n=5).

DP voltammograms over the concentration range from 1.0 to 100.0 ppb TNT and the corresponding calibration plot are illustrated in **Fig 7**. Data fitted the equation I(μA) =(0.0137±0.0002)[TNT(ppb)]−(0.0043±0.0020) with a coefficient of determination R^2=0.9989. The detection limit (LOD) based on the 3σ/m criterion [where σ, the standard deviation of the blank and m, the slope of the calibration plot] was calculated to be 0.44 ppb TNT.

3.7.2. Indirect electro oxidation of TNT

The response of sparked GNM−SPEs with respect to the electrochemical treatment at −0.275 V was investigated at different time intervals from 10 to 300 s (**Fig. S10**). A time of 120 s was selected as a compromise between sensitivity and total time of analysis. **Fig. 8** depicts the anodic DP voltammograms of GNM−SPEs at standard solutions of the target in 0.1 M PBS, pH 7 and the respective calibration plot showing a linear response over the concentration range from 1 to 50 ppb TNT. The equation for the straight line was I(μA)=(0.0421±0.0016)[TNT(ppb)]+(0.0041±0.0035) with a coefficient of determination R^2=0.9930. The inter electrode reproducibility among different electrodes was <4% (10 ppb TNT, n=5). The LOD based on the 3σ/m criterion was calculated to be 0.25 ppb TNT.

Comparison of the basic analytical figures of merit of sparked GNM−SPEs and other reported electrodes (**Table 1**) reveals that GNM−SPEs compare favorably to [13,17] and outperform other works based on complicated electrode buildups [7,9,20–22,24,25,31,33,34,10–12,14–16,18,19] and/or noble metal nanoparticles [9–11,20,31,34].

3.7.3 Application to real samples

Sparked GNM−SPEs were used for the determination of TNT in drinking water samples collected from the tap in the laboratory. The original concentration of TNT in the samples was nil or lower than the detection limit of the method and thus the samples were fortified with 2 or 10 ppb TNT. The recovery of the method at both the cathodic and anodic assay protocols described above was evaluated by using the standard addition method. Results are presented in **Table 2**.

4. Conclusions

3D−sparking head aided SPE−to−graphite pencil in−situ tailoring of low cost screen-printed electrodes results in the generation of sponge−like graphite nanostructures and low dimensional few−layer graphite flakes that endow SPE with outstanding electrocatalytic properties towards the electro-reduction of TNT in deoxygenated solutions.

The entire modification process requires an extremely low cost instrumentation and can be implemented in the absence of organic solvents, strong acids or any templates or specific reagents which are commonly used to the preparation of various nanomaterials, within a few minutes at a highly reproducible manner.

The cathodic determination of TNT allows an LOD as low as 0.44 ppb, while the tolerance ratio of the method towards the interference of 2,4−DNT is 25.

Graphite−sparked SPEs show also remarkable electrocatalytic properties to the anodic determination of TNT at non-deoxygenated solutions by measuring the oxidation of the electrochemically generated hydroxylamine groups at electrodes which have been prior polarized at −0.275 V for 2 min. At the cost of a slightly longer time of analysis, the anodic indirect determination of TNT offers the ability of use at on−site applications where purging of the sample is an obstacle, lower LOD of 0.25 ppb and interference free measurements in the presence of up to 50−fold higher concentration of 2,4−DNT.

Both cathodic and anodic electroanalytical formats were successfully applied to the determination of TNT at the ppb concentration level at spiked drinking water samples.

Credit author statement

Maria G. Trachioti: Investigation, Writing - original draft. **Dusan Hemzal:** Data curation-formal analysis. **Jan Hrbac:** Writing - review & editing**. Mamas I. Prodromidis:** Conceptualization, Supervision**,** Funding acquisition**,** Writing-Reviewing and Editing.

Declaration of interests

The authors declare that they have no known competing financial interests or personal relationships that could have appeared to influence the work reported in this paper.

References

[1] E. Mistek, M.A. Fikiet, S.R. Khandasammy, I.K. Lednev, Toward Locard's Exchange Principle: Recent Developments in Forensic Trace Evidence Analysis, Anal. Chem. 91 (2019) 637–654.

[2] S. Giannoukos, B. Brkić, S. Taylor, A. Marshall, G.F. Verbeck, Chemical Sniffing Instrumentation for Security Applications, Chem. Rev. 116 (2016) 8146–8172.

[3] State of California, Environmental Protection Agency, Office of Environmental Health Hazzard Assessment, Safe Drinking Water and Toxic Enforcement Act of 1986, September 2019, Chemicals known to the state to cause canser or reproductive toxicity.

[4] United States Environmetal Protection Agency (EPA), Office of Land and Emergency Management, November 2017, Technical fact sheet_2,4,6-trinitrotoluene (TNT).

[5] R.K. Mishra, A. Martín, T. Nakagawa, A. Barfidokht, X. Lu, J.R. Sempionatto, K.M. Lyu, A. Karajic, M.M. Musameh, I.L. Kyratzis, J. Wang, Detection of vapor-phase organophosphate threats using wearable conformable integrated epidermal and textile wireless biosensor systems, Biosens. Bioelectron. 101 (2018) 227–234.

[6] J.R. Sempionatto, R.K. Mishra, A. Martín, G. Tang, T. Nakagawa, X. Lu, A.S. Campbell, K.M. Lyu, J. Wang, Wearable Ring-Based Sensing Platform for Detecting Chemical Threats, ACS Sensors. 2 (2017) 1531–1538.

[7] R. Cánovas, M. Parrilla, P. Mercier, F.J. Andrade, J. Wang, Balloon-Embedded Sensors Withstanding Extreme Multiaxial Stretching and Global Bending Mechanical Stress: Towards Environmental and Security Monitoring, Adv. Mater. Technol. 1 (2016) 1–11.

[8] R.K. Mishra, L.J. Hubble, A. Martín, R. Kumar, A. Barfidokht, J. Kim, M.M. Musameh, I.L. Kyratzis, J. Wang, Wearable Flexible and Stretchable Glove Biosensor for On-Site Detection of Organophosphorus Chemical Threats, ACS Sensors. 2 (2017) 553–561.

[9] Ş. Sağlam, A. Üzer, E. Erçağ, R. Apak, Electrochemical Determination of TNT, DNT, RDX, and HMX with Gold Nanoparticles/Poly(Carbazole-Aniline) Film-Modified Glassy Carbon Sensor Electrodes Imprinted for Molecular Recognition of Nitroaromatics and Nitramines, Anal. Chem. 90 (2018) 7364–7370.

[10] Ş. Sağlam, A. Üzer, Y. Tekdemir, E. Erçağ, R. Apak, Electrochemical sensor for nitroaromatic type energetic materials using gold nanoparticles/poly(o-phenylenediamine-aniline) film modified glassy carbon electrode, Talanta. 139 (2015) 181–188.

[11] B. Filanovsky, B. Markovsky, T. Bourenko, N. Perkas, R. Persky, A. Gedanken, D. Aurbach, Carbon Electrodes Modified with TiO_2/Metal Nanoparticles and Their Application to the Detection of Trinitrotoluene, Adv. Funct. Mater. 17 (2007) 1487–1492.

[12] S.V.F. Castro, M.N.T. Silva, T.F. Tormin, M.H.P. Santana, E. Nossol, E.M. Richter, R.A.A. Munoz, Highly-sensitive voltammetric detection of trinitrotoluene on reduced graphene oxide/carbon nanotube nanocomposite sensor, Anal. Chim. Acta. 1035 (2018) 14–21.

[13] X. Ran, Q. Qu, X. Qian, W. Xie, S. Li, L. Li, L. Yang, Water-soluble pillar[6]arene functionalized nitrogen-doped carbon quantum dots with excellent supramolecular recognition capability and superior electrochemical sensing performance towards TNT, Sensors Actuators, B Chem. 257 (2018) 362–371.

[14] Y.T. Yew, A. Ambrosi, M. Pumera, Nitroaromatic explosives detection using electrochemically exfoliated graphene, Sci. Rep. 6 (2016) 1–11.

[15] S.M. Tan, C.K. Chua, M. Pumera, Graphenes prepared from multi-walled carbon nanotubes and stacked graphene nanofibers for detection of 2,4,6-trinitrotoluene (TNT) in seawater, Analyst. 138 (2013) 1700–1704.

[16] B.K. Ong, H.L. Poh, C.K. Chua, M. Pumera, Graphenes Prepared by Hummers, Staudenmaier and Hofmann Methods for Analysis of TNT-Based Nitroaromatic Explosives in Seawater, Electroanalysis. 24 (2012) 2085–2093.

[17] L. Zhang, Y. Han, J. Zhu, Y. Zhai, S. Dong, Simple and Sensitive Fluorescent and Electrochemical Trinitrotoluene Sensors Based on Aqueous Carbon Dots, Anal. Chem. 87 (2015) 2033–2036.

[18] M.S. Goh, M. Pumera, Graphene-based electrochemical sensor for detection of 2,4,6-trinitrotoluene (TNT) in seawater: the comparison of single-, few-, and multilayer graphene nanoribbons and graphite microparticles, Anal. Bioanal. Chem. 399 (2011) 127–131.

[19] T.H. Seah, H.L. Poh, C.K. Chua, Z. Sofer, M. Pumera, Towards Graphane Applications in Security: The Electrochemical Detection of Trinitrotoluene in Seawater on Hydrogenated Graphene, Electroanalysis. 26 (2014) 62–68.

[20] R. Zhang, C.L. Sun, Y.J. Lu, W. Chen, Graphene Nanoribbon-Supported PtPd Concave Nanocubes for Electrochemical Detection of TNT with High Sensitivity and Selectivity, Anal. Chem. 87 (2015) 12262–12269.

[21] S. Hrapovic, E. Majid, Y. Liu, K. Male, J.H.T. Luong, Metallic Nanoparticle-Carbon Nanotube Composites for Electrochemical Determination of Explosive Nitroaromatic Compounds, Anal. Chem. 78 (2006) 5504–5512.

[22] S. Guo, D. Wen, Y. Zhai, S. Dong, E. Wang, Platinum Nanoparticle Ensemble-on-Graphene Hybrid Nanosheet: One-Pot, Rapid Synthesis , and Used as New Electrode Material for Electrochemical Sensing, ACS Nano. 4 (2010) 3959–3968.

[23] F. Shahdost-fard, M. Roushani, Designing an ultra-sensitive aptasensor based on an AgNPs/thiol-GQD nanocomposite for TNT detection at femtomolar levels using the electrochemical oxidation of Rutin as a redox probe, Biosens. Bioelectron. 87 (2017) 724–731.

[24] D. Zhang, J. Jiang, J. Chen, Q. Zhang, Y. Lu, Y. Yao, S. Li, G. Logan Liu, Q. Liu, Smartphone-based portable biosensing system using impedance measurement with printed electrodes for 2,4,6-trinitrotoluene (TNT) detection, Biosens. Bioelectron. 70 (2015) 81–88.

[25] S.A. Trammell, D. Zabetakis, M. Moore, J. Verbarg, D.A. Stenger, Square Wave Voltammetry of TNT at Gold Electrodes Modified with Self-Assembled Monolayers Containing Aromatic Structures, PLoS One. 9 (2014) 1–12.

[26] M.G. Trachioti, E.I. Tzianni, D. Riman, J. Jurmanova, M.I. Prodromidis, J. Hrbac, Extended coverage of screen-printed graphite electrodes by spark discharge produced gold nanoparticles with a 3D positioning device. Assessment of sparking voltage-time characteristics to develop sensors with advanced electrocatalytic properties, Electrochim. Acta. 304 (2019) 292–300.

[27] V.A. Gatselou, D.L. Giokas, A.G. Vlessidis, M.I. Prodromidis, Rhodium nanoparticle-modified screen-printed graphite electrodes for the determination of hydrogen peroxide in tea extracts in the presence of oxygen, Talanta. 134 (2015) 482–487.

[28] M.C. Sousa, J.W. Buchanan, Observational Models of Graphite Pencil Materials, Comput. Graph. Forum. 19 (2000) 27–49.

[29] A.C. Ferrari, Raman spectroscopy of graphene and graphite: Disorder, electron-phonon coupling, doping and nonadiabatic effects, Solid State Commun. 143 (2007) 47–57.

[30] M.G. Trachioti, A.E. Karantzalis, J. Hrbac, M.I. Prodromidis, Low-cost screen-printed sensors on-demand: Instantly prepared sparked gold nanoparticles from eutectic Au/Si alloy for the determination of arsenic at the sub-ppb level, Sensors Actuators, B Chem. 281 (2019) 273–280.

[31] C. Tan, M.Z.M. Nasir, A. Ambrosi, M. Pumera, 3D Printed Electrodes for Detection of Nitroaromatic Explosives and Nerve Agents, Anal. Chem. 89 (2017) 8995–9001.

[32] C.K. Chua, M. Pumera, L. Rulíšek, Reduction Pathways of 2,4,6-Trinitrotoluene: An Electrochemical and Theoretical Study, J. Phys. Chem. C. 116 (2012) 4243–4251.

[33] J.S. Caygill, S.D. Collyer, J.L. Holmes, F. Davis, S.P.J. Higson, Disposable screen-printed sensors for the electrochemical detection of TNT and DNT, Analyst.

138 (2013) 346–352.

[34] R.G. Bozic, A.C. West, R. Levicky, Square wave voltammetric detection of 2,4,6-trinitrotoluene and 2,4-dinitrotoluene on a gold electrode modified with self-assembled monolayers, Sensors Actuators, B Chem. 133 (2008) 509–515.

Biographies

Maria Trachioti is a first year Ph.D candidate in the Laboratory of Analytical Chemistry of the University of Ioannina. She is majoring in the generation of metal or carbon-based nanomaterials by electrical discharge and the development of low-cost, disposable screen-printed chemical sensors for on-site applications.

Dr. Dusan Hemzal obtained his M.Sc. and Ph.D. degrees in Theoretical Physics at Masaryk university in Brno, Czech Republic. His current work deals with plasmon-enhanced Raman spectroscopy (SERS, TERS) and ellipsometry (TIRE) and their applications in biophysics, his research interests include also nanoparticle synthesis. He has 27 publications and has supervised 28 MSc. and/or BSc. students. He has been a visiting research fellow to Johannes Kepler Univeriisty in Linz (Austria) and Kyung-Hee university in Seoul (South Korea). His is currently a Researcher at CEITEC, Masaryk University.

Dr. Jan Hrbac obtained the M.Sc. and Ph.D. degrees in Chemistry at Palacky University in Olomouc, Czech Republic. His work deals with the design of modified electrodes and microelectrodes and their batch and flow electroanalytical applications. His research interests include also development and construction of electrochemical detector cells, electronics and programming. He has published more than 70 publications in peer-reviewed journals, one book chapter, holds three patents and one utility model. He has supervised 15 MSc. and 3 Ph.D. students and he has been visiting research fellow in Hebrew University of Jerusalem, Israel and NCSR Demokritos, Greece. He is currently Associate Professor of Physical Chemistry in Masaryk University.

Prof. Mamas I. Prodromidis obtained the B.Sc and Ph.D degrees in Chemistry at UoI and he is a Professor of Analytical Chemistry at UoI. His research interest focused on the development of electrochemical sensors and biosensors, the production of nanoparticles with spark discharge, the development of low-cost analytical devices for point-of-care analysis, on bipolar electrochemistry, and the design & fabrication of screen-printing electrodes and electrochemical cells. He has published more than 97 publications in peer-reviewed journals, four review articles, three book chapters and he also holds one patent. He has given more than 16 invited talks in seminars and international conferences, and he has been visiting researcher/professor in several Universities in Italy, UK, Germany, Spain and Miami.

FIGURE CAPTIONS

Fig. 1. (A, B) SEM images and (C) EDX mapping of carbon flakes which were extracted after the electric discharge between the SPE and the 2B Faber−Castell pencil at 1.2 kV under ambient conditions.

Fig. 2. (Top row) Raman imaging and (bottom row) representative Raman spectra of (A) plain, (B) sparked SPEs, and (C) spark−extracted carbon flake over the electrode substrate. Images for plain and sparked electrodes represent an area 30 μm x 30 μm. Imaging of the extracted flake (7 μm x 7 μm) uses additionally the substrate (PES) peaks in the gray channel (**Fig. S1**).

Fig. 3. (A) CVs and (B) Nyquist plots of the (black line) plain and sparked modified SPEs after (blue line) 43 and (red line) 203 sparking cycles at 0.1 M PBS, pH 7 containing (A) 5 mM hecacyanoferrate(III) and (B) 5+5 mM hecacyanoferrate(II)/(III).

Fig. 4. DP voltammograms of GNM−SPEs (graphite pencil 2B, 100 sparking cycles) in single solutions of various nitro aromatic compounds. Electrolyte, 0.1 M PBS, pH 7; concentration of compounds, 350 ppb; deposition potential, 0 V; deposition time, 10 s.

Fig. 5. CVs of GNM−SPEs (graphite pencil 2B, 203 sparking cycles) in single solutions of various nitro aromatic compounds. Electrolyte, 0.1 M PBS, pH 7; concentration of compounds, 10^{-5} M; CVs show the 2nd scan; starting potential, 0 V.

Fig. 6. DP voltammograms of GNM−SPEs in (black line) 0.1 M PBS, pH 7, (red line) 0.1 M PBS, pH 7 containing 625 ppb 2,4−DNT and in (blue line) 0.1 M PBS, pH 7 containing 625 ppb 2,4−DNT and 25 ppb TNT after the application of different treatment potential values at (a) −250, (b) −275, (c) −300 and (d) −325 mV. Application time, 10 s.

Fig. 7. DP voltammograms of GNM−SPE in 0.1 M PBS, pH 7 containing 0, 1, 2, 5, 10, 25, 50, 75 and 100 ppb TNT and the respective calibration plot (inset). All measurements were contacted with a single electrode.

Fig. 8. DP voltammograms of GNM−SPEs in 0.1 M PBS, pH 7 containing 0, 1, 2, 5, 10, 25 and 50 ppb TNT and the respective calibration plot (inset). Each measurement was conducted with a new electrode after a cathodic treatment at −275 mV for 120 s.

Table 1. Comparison of the major analytical figure of merits of sparked GNM−SPEs with other published methods on the electrochemical determination of TNT.

Electrode	Linear range (ppb)	LOD (ppb)	Ref.
AuNP/poly(CA)−GCE	100−1000	25	[9]
rGO/MWCNT−BDE	114−250000	4.32	[12]
Gold−plated 3D electrode	50000−100000	n.p	[31]
Balloon−embedded sensor	20−100	n.p	[7]
Carbon SPEs	227−45455	90.9	[33]
AuNP/poly(o−PD−aniline)−GCE	2500−40000	2100	[10]
PtPd−rGONRs	10−3000	0.8	[20]
GC/Cu_{nano}/SWCNT + Nafion	1−2000	1	[21]
PNEGHN/GCE	500−40000	300	[22]
RDE(Au)−SAM	12−120	3	[34]
WP6−N−CQD/GCE	0.23−227.3 227.3−4545	0.22	[13]
TNT−peptide−SPE	227−227273	159.1	[24]
TiO_2/nano−Pt(Au)(Ru)−CPE	3000−5000	2000	[11]
AuE−SAM	0−10000	500	[25]
EEGS−GCE	4000−20000	2030	[14]
GSs−GCE	4000−20000	140	[15]
G−GCE	4000−20000	n.p	[16]
CDs−GCE	1−6818	0.23	[17]
GNR(Ms)−GCE	1000−15000	1000	[18]
TRG−GCE	4000−20000	400	[19]
Graphite pencil−sparked SPE (cathodic mode)	1−100	0.44	This work
Graphite pencil−sparked SPE (anodic mode)	1−50	0.25	

Key: AuNP/poly(CA)−GCE, gold nanoparticle/poly(carbazole−aniline)−modified GCE; rGO/MWCNT−BDE, reduced graphene oxide/multi−walled carbon nanotube−modified boron−doped diamond electrode; AuNP/poly(o−PD−aniline)−GCE, gold nanoparticle /poly(o−phenylenediamine−aniline)−modified GCE; PtPd−rGONRs−GCE, graphene nanoribbon−supported PtPd concave nanocubes−modified GCE; GC/Cu_{nano}/SWCNT + Nafion, copper nanoparticle/single−walled carbon nanotubes solubilized in Nafion−modified GCE; PNEGHN/GCE, platinum nanoparticle ensemble−on−graphene hybrid nanosheet/Nafion modified GCE; RDE(Au)−SAM, rotating disc gold electrode, modified with an alkanethiol self−assembled monolayer; WP6−N−CQD/GCE, water−soluble pillar arene functionalized nitrogen−doped carbon quantum dots modified GCE; TiO_2/nano−Pt(Au)(Ru)−CPE, composites of nanometer-sized mesoporous titanium dioxide containing inserted/deposited ruthenium, platinum or gold nanoparticle modified carbon−paper electrode; AuE−SAM, gold electrodes modified with alkane thiol or aromatic ring thiol self-assembled monolayers; EEGS−GCE, GCE modified with electrochemically exfoliated graphene sheets; GSs-GCE, GCE modified with GSs prepared from MWCNTs and stacked graphene nanofibers; G−GCE, thermally exfoliated graphene prepared by Hummers, Staudenmaier or Hofmann methods; CDs−GCE, GCE modified with aqueous N−rich carbon dots; GNR(Ms)−GCE, single−, few−, multilayer graphene nanoribbons or graphite microparticle−based GCE; TRG−GCE, GCE modified with thermally reduced graphene. n.p, not provided.

Table 2: Recovery of TNT in spiked tap water samples. Values show the mean value and the standard deviation of three measurements.

Sample	Amount added, ppb	Amount determined, ppb	Recovery, %	RSD, %
A	0	0		
cathodic	2	2.15 ± 0.16	108	7.4
A	0	0		
anodic	2	2.03 ± 0.07	102	3.5
B	0	0		
cathodic	10	10.07 ± 0.85	101	7.9

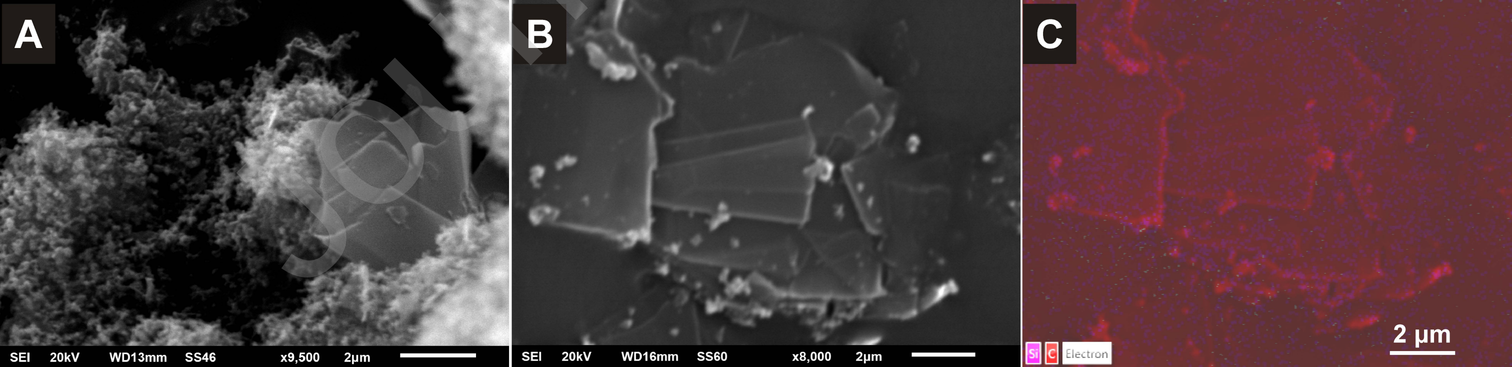
A
B
C
SEI 20kV WD13mm SS46 x9,500 2μm
SEI 20kV WD16mm SS60 x8,000 2μm
2 μm
Si
C
Electron

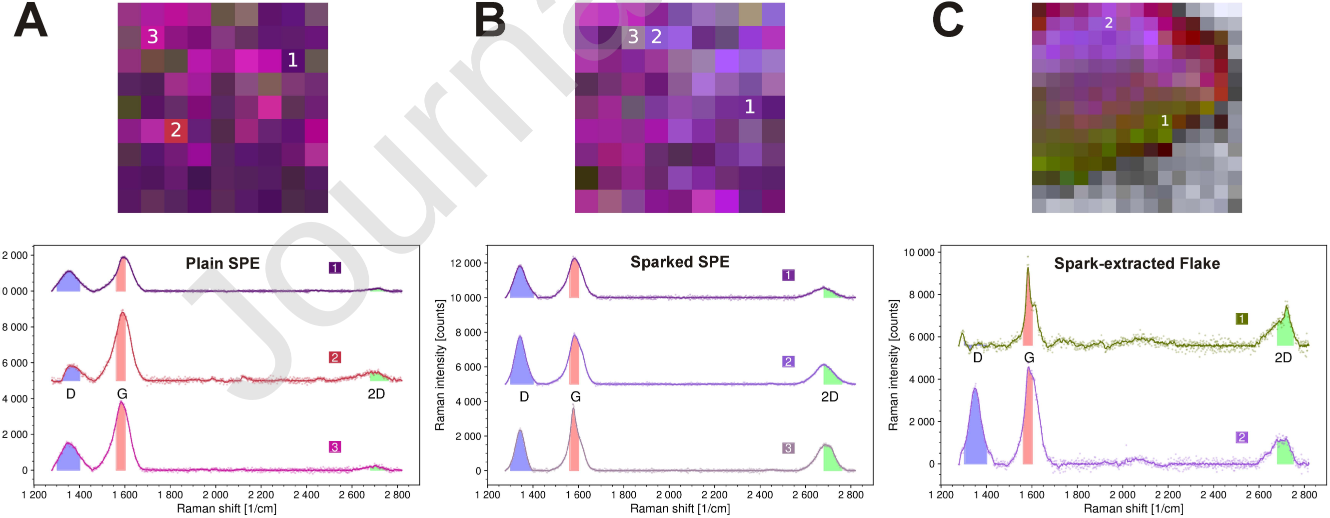
A
3
1
2
B
3
2
1
C
2
1
Plain SPE
1
2
3
D
G
2D
Sparked SPE
1
2
3
D
G
2D
Spark-extracted Flake
1
2
D
G
2D
Raman intensity [counts]
Raman shift [1/cm]
12 000
10 000
8 000
6 000
4 000
2 000
0
1 200
1 400
1 600
1 800
2 000
2 200
2 400
2 600
2 800

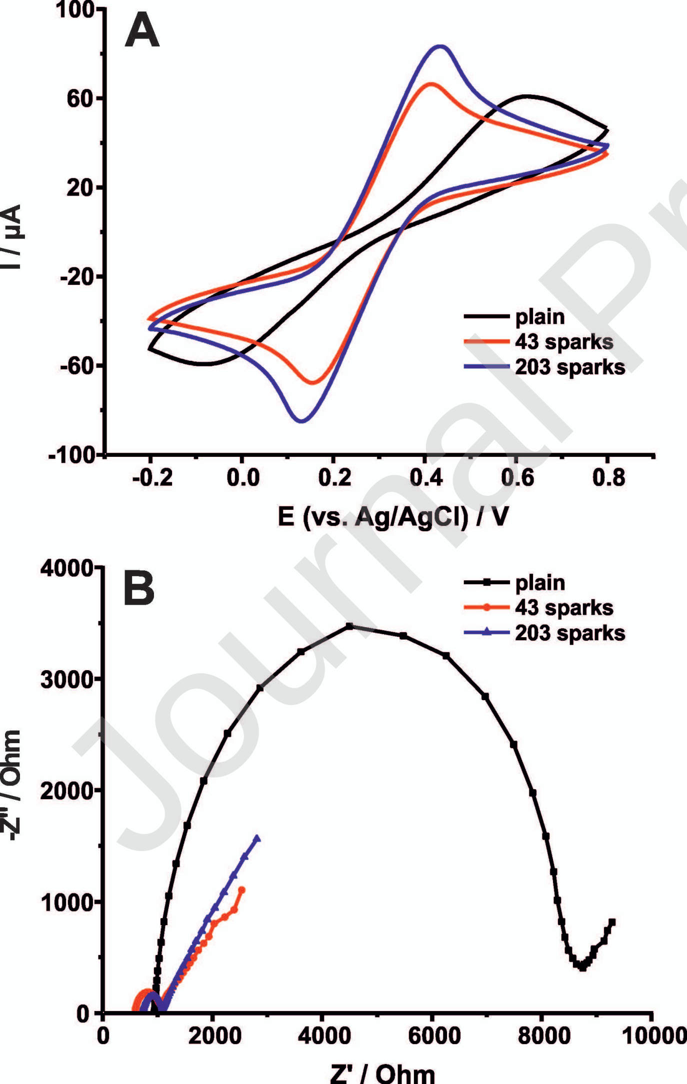
A
100
60
20
-20
-60
-100
I / µA
-0.2
0.0
0.2
0.4
0.6
0.8
E (vs. Ag/AgCl) / V
plain
43 sparks
203 sparks
B
4000
3000
2000
1000
0
-Z'' / Ohm
0
2000
4000
6000
8000
10000
Z' / Ohm
plain
43 sparks
203 sparks

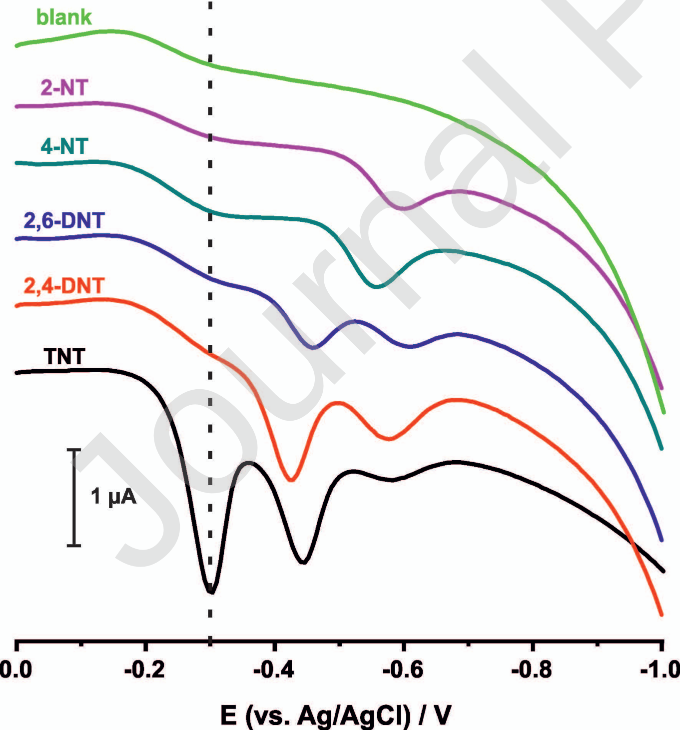
blank
2-NT
4-NT
2,6-DNT
2,4-DNT
TNT
1 µA
0.0
-0.2
-0.4
-0.6
-0.8
-1.0
E (vs. Ag/AgCl) / V

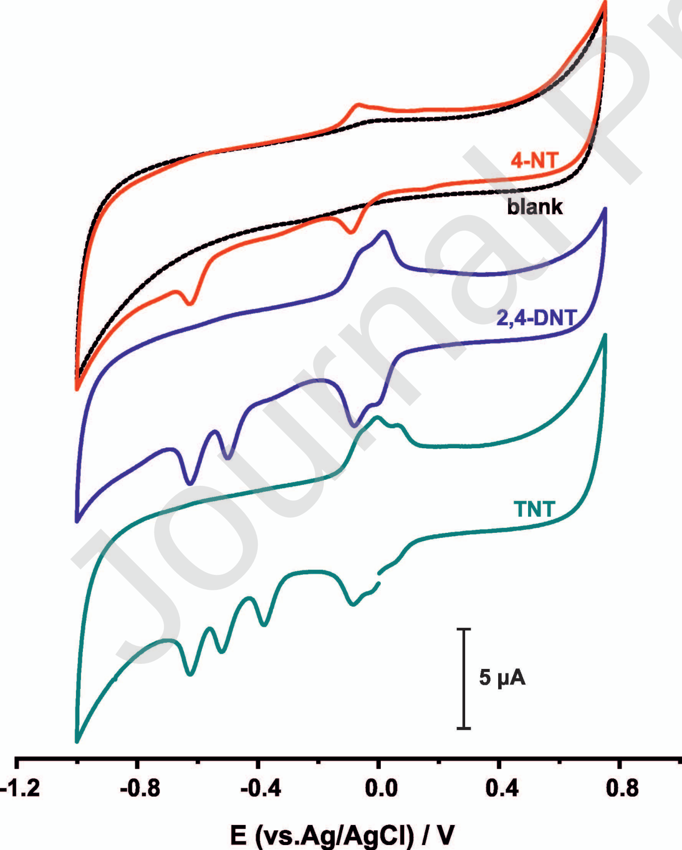
4-NT
blank
2,4-DNT
TNT
5 μA
-1.2
-0.8
-0.4
0.0
0.4
0.8
E (vs.Ag/AgCl) / V

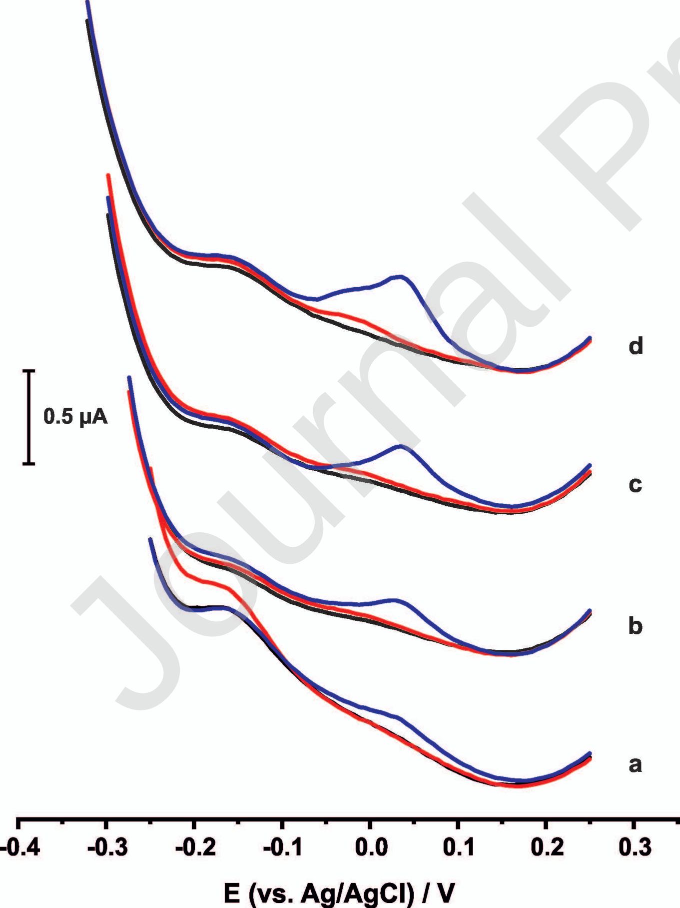
d
c
b
a
0.5 µA
-0.4
-0.3
-0.2
-0.1
0.0
0.1
0.2
0.3
E (vs. Ag/AgCl) / V

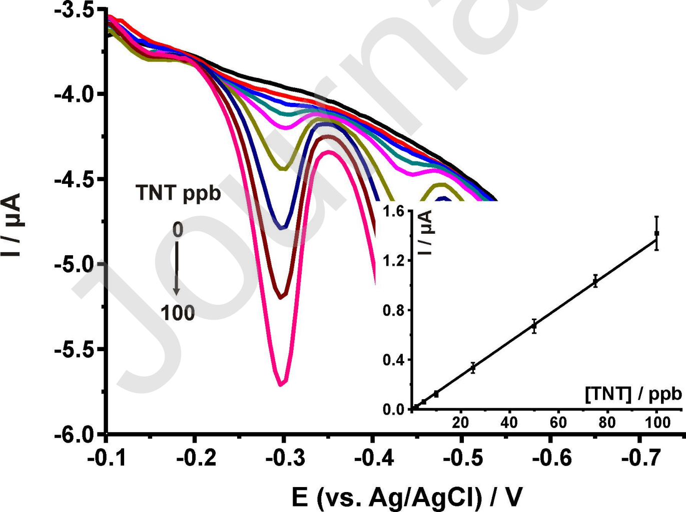
-3.5
-4.0
-4.5
-5.0
-5.5
-6.0
I / µA
TNT ppb
0
100
-0.1
-0.2
-0.3
-0.4
-0.5
-0.6
-0.7
E (vs. Ag/AgCl) / V
1.6
1.2
0.8
0.4
0.0
I / µA
[TNT] / ppb
20
40
60
80
100

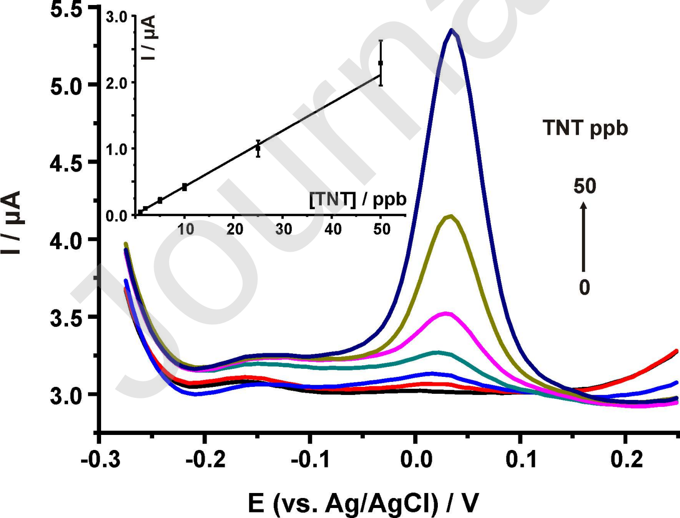
I / µA
5.5
5.0
4.5
4.0
3.5
3.0
-0.3
-0.2
-0.1
0.0
0.1
0.2
E (vs. Ag/AgCl) / V
TNT ppb
50
0
I / µA
3.0
2.0
1.0
0.0
10
20
30
40
50
[TNT] / ppb